JCTC Journal of Chemical Theory and Computation

Article

pubs.acs.org/JCTC

Constant Pressure Path Integral Gibbs Ensemble Monte Carlo Method

Piotr Kowalczyk,*[,†] Piotr A. Gauden,[‡] Artur P. Terzyk,[‡] Evangelia Pantatosaki,[§] and George K. Papadopoulos[§]

[†]Nanochemistry Research Institute, Department of Chemistry, Curtin University of Technology, P.O. Box U1987, Perth, 6845 Western Australia, Australia

[‡]Department of Chemistry, Physicochemistry of Carbon Materials Research Group, N. Copernicus University, Gagarin St. 7, 87-100 Torun, Poland

[§]School of Chemical Engineering, National Technical University of Athens, 9 Heroon Polytechniou Street, 157 80 Athens, Greece

Supporting Information

ABSTRACT: We present the implementation of a real-space constant pressure path integral Gibbs ensemble Monte Carlo (CP-PIGEMC) method for the simulation of one-component fluid consists of distinguishable quantum particles (henceforth referred to as *Boltzmannons*) in an external potential field at finite temperatures. We apply this simulation method to study the *para*-H_2 adsorption in NaX zeolite at 77 K and pressures up to 100 bar. We present a new set of effective solid−fluid parameters optimized for path integral simulations of hydrogen isotope adsorption and separation in synthetic zeolites. The agreement among CP-PIGEMC, experiment, and the path integral grand canonical Monte Carlo method (PIGCMC) is very good, even at high pressures. CP-PIGEMC is a particularly useful method for simulation of one-component quantum fluid composed of Boltzmannons at finite temperatures, when the chemical potential is difficult to measure or calculate explicitly.

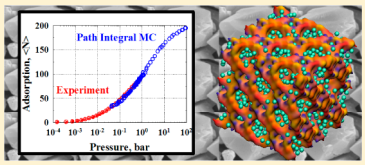

I. INTRODUCTION

Since its original formulation in 1948,[1,2] Feynman's space−time approach to nonrelativistic quantum mechanics (known as 'path integral' or 'sum over histories') has provided a powerful tool for studying many-body problems at finite temperatures without introducing uncontrolled approximations.[3−22] While computing thermodynamic properties of homogeneous quantum fluids (in this study "quantum fluids" are restricted to fluids composed of Boltzmannons) at finite temperatures via path integral has become routine,[3,4] the calculation of thermodynamic properties of an open isothermal system (i.e., a system that can exchange both heat energy and quantum particles with its surroundings) remains a challenging problem in computational chemistry. Adsorption of light particles (i.e., hydrogen isotopes, light noble gases, and light alkanes) in nanoporous materials at cryogenic temperatures is a typical example, where the simulation in an open system offers a natural framework for calculation of basic thermodynamic functions (i.e., the amount of adsorbed fluid, the enthalpy accompanying the adsorption processes, etc.).

To the best of our knowledge, there are two primary force-field based techniques for the simulation of the equilibrium properties of quantum fluids confined by an external field: path integral grand canonical Monte Carlo (PIGCMC)[23] and path integral gauge cell Monte Carlo (PIGMC).[24] Both methods of simulation use the quantum-classical isomorphism of Chandler and Wolynes,[25] where each quantum particle is represented by a classical cyclic 'ring polymer'. In PIGCMC the chemical potential, volume, and temperature are fixed. The external field is sampled by the random creation and destruction of quantum particles (Widom moves), whereas the thermalization of confined quantum particles is achieved by their random translations (Metropolis moves).[23] In PIGMC, the simulation system consists of two cells: gauge and external field (called also pore cell).[24] In each cell, quantum particles are thermalized by random translations, whereas the equality of the chemical potential in both cells is achieved by a so-called exchange step. Direct observation of metastable and unstable states of confined quantum particles at the atomistic level is an advantage of PIGMC over PIGCMC.[24,26,27]

In order to relate PIGCMC as well as PIGMC simulation results to experimental porosimetry or calorimetric measurements, the relation between the chemical potential and pressure of the studied quantum fluid has to be known.[23,24] For simple classical fluids (such as spherical particles), the pressure and chemical potential can be obtained with reasonable precision, but for quantum fluids at low temperatures, the process is difficult and less accurate. The original method of Widom (known as the particle insertion method)[28] implemented in canonical or Gibbs path integral ensemble is a standard technique used for the calculation of the chemical potential of a homogeneous quantum fluid.[6,23] This method is precise; however, approximations (i.e., types of estimators, number of beads per polymer chain, etc.) must be made if the pressure is to be calculated. Moreover, these path integral Monte Carlo

Received: February 11, 2013

   dx.doi.org/10.1021/ct400110c | J. Chem. Theory Comput. XXXX, XXX, XXX−XXX

simulation methods carry a relatively high memory and computational overhead if the studied homogeneous quantum fluid is dense.

Similarly to the classical grand canonical Monte Carlo mehod,[29] an accurate equation of state combined with PIGCMC estimation of bulk density is an alternative method for the relation of the chemical potential to bulk pressure. Although this methodology is very attractive, it can be only applied when an accurate equation of state is known for the studied quantum fluid and thermodynamic conditions. Besides, any PIGCMC simulation that involves study of fluids consisting of light particles at low temperatures is computationally expensive and time-consuming.

By taking into account these arguments, we argue that a novel path integral technique with pressure, volume, and temperature as input parameters, is an interesting alternative to the currently used path integral simulation algorithms. Therefore, we present the extension of the constant pressure Gibbs ensemble Monte Carlo method of McGrother and Gubbins[30] to simulations of confined quantum fluids. All computational details (including the description of simulation system, particle interactions, Monte Carlo perturbations, simulation details, and computed averages) are documented in paragraph II. We would like to stress that all Monte Carlo transition probabilities used in our CP-PIGEMC program have been rigorously derived by Wang and co-workers.[6,23] Next, we present the case study of N_2 adsorption−desorption in cylindrical silica pores at 77.4 K. For the first time, constant pressure Gibbs ensemble Monte Carlo and Grand Canonical Monte Carlo simulation algorithms implemented for the classical fluids are compared (see paragraph III and simulation results in the Supporting Information). Finally, in paragraph IV, we present the case study of *para*-H_2 (i.e., our model quantum fluid) adsorption in NaX zeolite crystal (i.e., our model nanoporous material) at 77 K. Here, our novel CP-PIGEMC algorithm has been validated against experimental measurements and simulation data computed from the well-established PIGCMC[10] simulation method.

II. COMPUTATIONAL DETAILS

II.1. Simulation System. We consider the thermodynamic equilibrium between the bulk and adsorbed one-component fluid of quantum particles. As we pointed out, we restrict our study to quantum particles that obey Boltzmann statistics. We assume further that quantum particles are spherical and spineless. To study the thermodynamic equilibrium between bulk and adsorbed one-component quantum fluid, we construct the simulation system consisting of two cells: bulk (subscript "b") and pore (subscript "p") cell, as is schematically shown in Figure 1. Both simulation cells are embedded in an infinitely large heat bath at temperature T, but they are not in physical contact. The number of quantum particles, N, and the volume of the pore cell, V_p, of the simulation system are fixed. The volume of the bulk cell, V_b, that represents bulk quantum fluid coexisting with the pore cell is not fixed. It fluctuates to ensure the equilibration of the assumed bulk pressure. In each cell, quantum particles are thermalized independently. The equality of the chemical potential in both cells is achieved by an exchange of quantum particles.

The expressions for the Monte Carlo (MC) acceptance probabilities (i.e., MC perturbation moves) require definitions of particle interactions in both bulk and pore simulation cells. Thus, in section II.2, we present a detailed description of these interactions. Finally, in section II.3, we provide the expressions for the Monte Carlo acceptance probabilities used in our CP-PIGEMC simulation algorithm with additional simulation details.

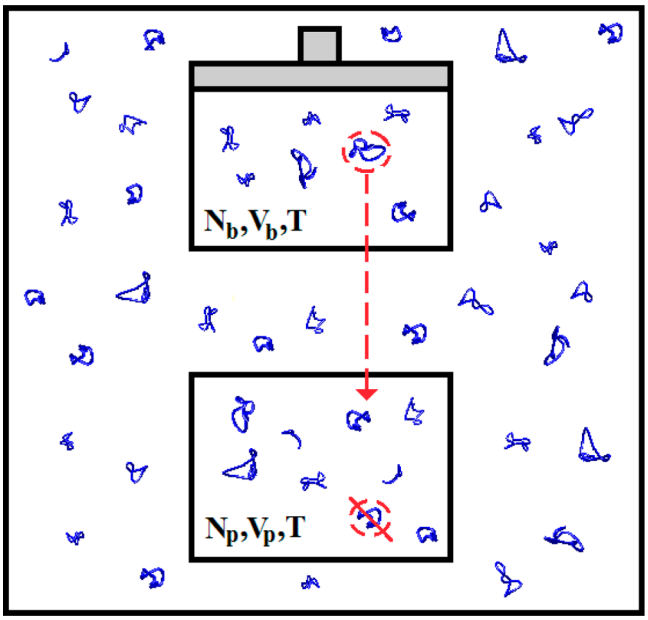

Figure 1. Schematic view of the simulation system: pore and bulk cell are in thermal equilibrium with a heat bath at temperature T. The bulk cell can exchange volume with the surroundings via isotropic expansion or contraction. The pore cell and bulk cell can exchange quantum particles (see blue cyclic paths), but quantum particles cannot transfer from or to the surroundings, $N_p + N_b = N = \text{const}$.

II.2. Particle Interactions (Primitive Approximation). Following Feynman's path integral formulation of quantum statistical mechanics,[1,2] we mapped each quantum particle onto an equivalent polymer chain or "necklace" of P classical "beads" $\mathbf{r}_i^{(1)},\mathbf{r}_i^{(2)},...,\mathbf{r}_i^{(p)}$. The vector $\mathbf{r}$ denotes the position of a bead belonging to the i-th particle. In the bulk cell (i.e., simulation cell that represents the homogeneous bulk quantum fluid), we compute the total potential energy from the primitive approximation given by[3,4]

$$E_b = E_b^{int} + E_b^{ext} \tag{1}$$

$$E_b^{int} = \frac{mP}{2(\beta\hbar)^2}\sum_{i=1}^{N_b}\sum_{k=1}^{P}|\mathbf{r}_i^k - \mathbf{r}_i^{k+1}| \tag{2}$$

$$E_b^{ext} = \frac{1}{P}\sum_{i<j}\sum_{k=1}^{P}\phi_{f-f}(r_{ij}^k) \tag{3}$$

where $r_{ij}^k = |\mathbf{r}_i^k - \mathbf{r}_j^k|$, N_b is the number of quantum particles in the bulk cell, $\beta = (k_B T)^{-1}$ is the inverse of thermal energy, m denotes the mass of the particle, and $\hbar = h/2\pi$ is Planck's constant. Owing to the cyclic condition of the polymer chains, if $k = P$, then $k + 1 = 1$.

In the current study, we select *para*-H_2 as model quantum fluid. We employ the widely used Silvera−Goldman (SG) potential for the calculation of the interactions between *para*-H_2 molecules:[31]

dx.doi.org/10.1021/ct400110c | J. Chem. Theory Comput. XXXX, XXX, XXX−XXX

$$\phi_{f-f}(r) = \exp(\alpha - \delta r - \gamma r^2) - \left(\frac{C_6}{r^6} + \frac{C_8}{r^8} + \frac{C_{10}}{r^{10}}\right) f_c(r) + \frac{C_9}{r^9} f_c(r) \quad (4)$$

where the first term on the right-hand side (RHS) accounts for short-range repulsive interactions, the second set of terms on the RHS account for long-range attractive dispersion interactions, and the last term on the RHS is an effective three-body correction. The last two terms are multiplied by a damping function, which turns off these interactions at short distances and is given by

$$f_C(r) = e^{-(r_c/r-1)^2}\theta(r_C - r) + \theta(r_C - r) \quad (5)$$

where $\theta(r)$ is the Heaviside function. The parameters for the SG potential are given in Table 1S in the Supporting Information. The isotropic SG potential has been found to provide a satisfactory agreement with experimental results.[12,31] The approximation of *para*-H_2 by isotropic model can be justified by the light mass of quantum rotor (i.e., for larger mass molecules, the moment of inertia is larger).

In the nanoporous materials, the potential acting on the adsorbed particles is the sum of fluid−fluid and solid−fluid interactions. Therefore, the total potential energy is given by the following primitive approximation:[18,23,24]

$$E_p = E_p^{int} + E_p^{ext} \quad (6)$$

$$E_p^{int} = \frac{mP}{2(\beta\hbar)^2} \sum_{i=1}^{N_p} \sum_{k=1}^{P} |\mathbf{r}_i^k - \mathbf{r}_i^{k+1}| \quad (7)$$

$$E_p^{ext} = \frac{1}{P} \sum_{i<j} \sum_{k=1}^{P} \phi_{f-f}(r_{ij}^k) + \frac{1}{P} \sum_{i=1}^{P} \sum_{k=1}^{N_s} \phi_{s-f}(r_{ik}) \quad (8)$$

where $r_{ik} = |\mathbf{r}_i - \mathbf{r}_k|$, N_p is the number of quantum particles in the pore cell, and N_s is the number of solid particles.

In the current study, we select NaX zeolite (i.e., the structure of a cubic NaX unit cell is $Na_{85}Al_{86}Si_{106},O_{384}$) as model nanoporous material. In treating the nanoporous material, we fix all solid particles at their crystallographic coordinates. We employ the widely used Kiselev approximation[32−34] to compute the interaction potential between the *para*-H_2 molecule and solid particles:

$$\frac{1}{P} \sum_{i=1}^{P} \sum_{k=1}^{N_s} \phi_{s-f}(r_{ik}) = \frac{1}{P} \sum_{i=1}^{P} \left[\sum_{k=1}^{N_{Si}} \phi_{Si-f}(r_{ik}) + \sum_{k=1}^{N_{Al}} \phi_{Al-f}(r_{ik}) + \sum_{k=1}^{N_O} \phi_{O-f}(r_{ik}) + \sum_{k=1}^{N_{Na}} \phi_{Na-f}(r_{ik})\right] \quad (9)$$

$$\phi_{Si-f}(r) = \begin{cases} \infty & \text{if } 0 < r < \sigma_{Si-f} \\ 0 & \text{if } r > \sigma_{Si-f} \end{cases} \quad (10)$$

$$\phi_{Al-f}(r) = \begin{cases} \infty & \text{if } 0 < r < \sigma_{Al-f} \\ 0 & \text{if } r > \sigma_{Al-f} \end{cases} \quad (11)$$

$$\phi_{O-f}(r) = 4\varepsilon_{O-f}\left[\left(\frac{\sigma_{O-f}}{r}\right)^{12} - \left(\frac{\sigma_{O-f}}{r}\right)^{6}\right] \quad (12)$$

$$\phi_{Na-f}(r) = 4\varepsilon_{Na-f}\left[\left(\frac{\sigma_{Na-f}}{r}\right)^{12} - \left(\frac{\sigma_{Na-f}}{r}\right)^{6}\right] \quad (13)$$

The Lennard-Jones potential parameters, $\sigma_{Na-f} = 2.8$ (Å), $\varepsilon_{Na-f}/k_B = 255$ (K), $\sigma_{O-f} = 2.8$ (Å), and $\varepsilon_{Na-f}/k_B = 45$ (K), were optimized to match the experimental adsorption isotherm of hydrogen in NaX zeolite measured at 77 K.[35,36] For hard-sphere potentials (eqs 10 and 11), we assumed $\sigma_{Si-f} = \sigma_{Al-f} = r_{min}$, where $r_{min} = 0.7\ \sigma_{H_2}$, and $\sigma_{H_2} = 2.958$ (Å). We would like to point out that these effective solid−fluid parameters should be used only in path integral simulations with the Kiselev force field approximation.

II.3. Monte Carlo Perturbations. *II.3.1. Particle Displacement.* In each cell, quantum particles are thermalized independently by random displacements. In our implementation, we used the simplest bead per bead sampling method. The path displacement perturbation consists of two steps. First, we move the entire randomly selected polymer chain by using centroid translation. Second, we perturb the position of a randomly selected bead in the displaced polymer chain.[10] New configuration of paths was accepted following the standard Metropolis algorithm:[37]

$$\text{acc}(s \rightarrow s') = \min\{1, \exp(-\beta \Delta E_j)\} \quad (14)$$

where $\Delta E_j = E_j(\mathbf{r}'^{N_j}) - E_j(\mathbf{r}^{N_j})$ is the change in the total potential energy of the path configuration in the selected simulation cell (where subscript "*j*" denotes selected simulation cell: "p" or "b") at the studied temperature (see eq 1 for the bulk cell, and eq 6 for the pore cell, respectively). Displacement step size is adjusted to give an acceptance ratio of 50% in each simulation cell. We would like to stress that other numerical algorithms (i.e., bisection, staging transformation, or normal-mode decomposition of the discretized action)[3,4,12,14] are superior sampling techniques. Monte Carlo staging algorithm[12,14] will be subject of our future code improvement.

II.3.2. Particle Exchange. The equality of the chemical potential in both cells is achieved by an exchange step implemented following the *ideal gas sampling method* of Wang and Johnson.[6,23] The conformation of the inserted quantum particle (i.e., the cyclic path) was chosen uniformly from the conformations of an ideal gas system. Practical implementation of this method is straightforward. First, we simulate a *para*-H_2 fluid consisting of 500 particles in the gas phase using canonical path integral Monte Carlo method. Second, we store path conformations into our database. In CP-PIGEMC simulation, we select uniformly the configuration of a trial inserted quantum particle from our database. The quantum particle for trial destruction is chosen uniformly from the selected cell. A trial transfer from the bulk cell (subscript "b") to the pore cell (subscript "p") is accepted with the probability:[6]

dx.doi.org/10.1021/ct400110c | J. Chem. Theory Comput. XXXX, XXX, XXX−XXX

$$\mathrm{acc}(s \rightarrow s') = \min\left\{1, \exp\left\{-\left(\beta\Delta E_b^{ext} + \beta\Delta E_p^{ext} + \ln\left[\frac{V_b(N_p+1)}{V_p N_b}\right]\right)\right\}\right\} \quad (15)$$

Note that the changes of the energy in the pore and bulk cell contain only the external part of the total energy (i.e., eq 3 and 8, see ref 6 for other details). In eq 15, V and N denote volume and number of quantum particles in "p" and "b" simulation cell, respectively. Clearly, the same rule (with changed subscripts) is applied to a trial transfer from the pore cell to the bulk cell.

II.3.3. Volume Change. The external pressure, p, in the bulk cell is equilibrated by the volume change move.[30] In this move, we scale intermolecular distances between quantum particles to accomplish an isotropic expansion or contraction. The intramolecular distances remain unchanged. Thus, only the external part of the total energy is changed during the perturbation of the bulk cell volume (i.e., eq 3, see ref 6 for other details). The new configuration of the bulk cell is accepted with the probability:[30,37]

$$\mathrm{acc}(s \rightarrow s') = \min\left\{1, \exp\left\{-\left(\beta\Delta E_b^{ext} + \beta p(V_b^{new} - V_b^{old}) - N_b \ln\left[\frac{V_b^{new}}{V_b^{old}}\right]\right)\right\}\right\} \quad (16)$$

where V_b^{new} and V_b^{new} denotes new and old volume of the bulk cell, respectively.

II.4. Simulation Details and Computed Averages. For many practical applications, the key adsorption data is specified by the temperature and external pressure of bulk fluid (for instance: 77 K and 1 bar).[38] Thus, we designed our CP-PIGEMC algorithm to simulate the specified adsorption point rather than continuous adsorption data.[29] To ensure microscopic reversibility, we used equal probability for displacement and quantum particle exchange moves. The volume change is attempted once per CP-PIGEMC cycle (where a cycle consists of N_b attempted perturbations of the old configuration in the bulk cell). In all CP-PIGEMC simulations, 5×10^7 cycles were generated, of which we discarded the first 1×10^7 to guarantee equilibration. All computed averages were fully reproducible in longer CP-PIGEMC runs. To save computational time, CP-PIGEMC averages were computed for selected adsorption points from single simulation runs.

The PIGCMC algorithm developed in ref 10 was used to generate reference thermodynamic data for *para*-H_2 adsorbed in NaX zeolite at 77 K. To calculate statistical error bars, we ran 15 independent PIGCMC simulations. Error bars were computed assuming a normal (Gaussian) distribution for the simulated values of averages. Additionally, we have performed a series of canonical (NVT) molecular dynamics simulations (MD) in order to compute the *para*-H_2 adsorption isotherm in NaX zeolite at 77 K. MD protocol, potential models, and simulation details can be found elsewhere.[35,39]

We computed the Gibbs absolute value of *para*-H_2 adsorption per NaX zeolite unit cell from the following equation:[10,29]

$$\Gamma = \langle N_p \rangle / V_c \quad (17)$$

where $\langle ... \rangle$ denotes the ensemble average and N_p is the number of *para*-H_2 molecules in the volume of a unit cell of NaX zeolite crystal, V_c.

To study the impact of confinement effects on the 'effective size' of *para*-H_2 molecules, we computed the radius of gyration from the following expression:[10]

$$\langle R_g \rangle = \sqrt{\left\langle \frac{1}{P}\sum_{i=1}^{P} |\mathbf{r}_i^t - \mathbf{R}_{CM,i}|^2 \right\rangle} \quad (18)$$

where $\mathbf{R}_{CM,i}$ is the centroid position of the i-th path. Note that the average given by eq 18 was collected in both the bulk cell and the pore cell, simultaneously. This allows straightforward analysis of the impact of confinement effects on the positional space localization of *para*-H_2 molecules.

To get more insight into the thermodynamics of *para*-H_2 adsorption, we computed the enthalpy of adsorption per mole from the thermodynamic estimator (known also as the Barker estimator):[40,41]

$$Q = \frac{5}{2}k_B T - \frac{3}{2}Pk_B T - \frac{\langle E_p^{ext} N_p \rangle - \langle E_p^{ext} \rangle \langle N_p \rangle}{\langle N_p^2 \rangle - \langle N_p \rangle^2} - \frac{\langle E_p^{int} \rangle \langle N_p \rangle - \langle E_p^{int} N_p \rangle}{\langle N_p^2 \rangle - \langle N_p \rangle^2} \quad (11)$$

were E_p^{int} and E_p^{ext} are given by eqs 7 and 8. All averages in eq 11 were computed on the fly, which eliminates any postsimulation analysis.

III. Classical Constant Pressure Gibbs Ensemble Monte Carlo Method. To the best of our knowledge, constant pressure Gibbs ensemble Monte Carlo simulation implemented for classical fluids has been never validated against the well-established grand canonical Monte Carlo simulation method. To fill this gap, we report N_2 adsorption−desorption isotherms and adsorption enthalpies in cylindrical silica pores at 77.4 K computed from both studied simulation algorithms (see simulation results attached in the Supporting Information).

IV. RESULTS AND DISCUSSIONS

We begin our discussion by considering the use of Boltzmann statistics in our path integral simulations of *para*-H_2 adsorption in NaX zeolite at 77 K. The presented CP-PIGEMC algorithm does not account for effects related to Bose statistics (i.e., exchanges of indistinguishable particles). It has been previously shown that Bose statistics has to be attached in path integral simulations when the degeneracy temperature, T_D, is close to the studied one.[3,4] Following Ceperley,[3] the degeneracy temperature can be computed from the following relation $T_D = \rho^{2/3}\hbar^2/mk_B$ (see eq 2.31 in ref 3), where ρ denotes density of studied quantum fluid. Even for a *para*-H_2 density of 40 mmol cm^{-3}, which is higher than the liquid density of *para*-H_2, T_D is around 2 K. This value of T_D is far below 77 K. Moreover, at the studied temperature, the de Broglie wavelength corresponding to hydrogen molecule, λ = 1.4 (Å), is smaller than the collision diameter of *para*-H_2 molecule, 2.958 (Å). We are thus confident that the Bose exchange effects can be disregarded and

dx.doi.org/10.1021/ct400110c | J. Chem. Theory Comput. XXXX, XXX, XXX−XXX

studied *para*-H_2 fluid (either in the bulk or adsorbed in NaX zeolite) is considered Boltzmann quantum fluid.

Figure 2 depicts a comparison between *para*-H_2 absolute Gibbs adsorption isotherms in NaX zeolite simulated

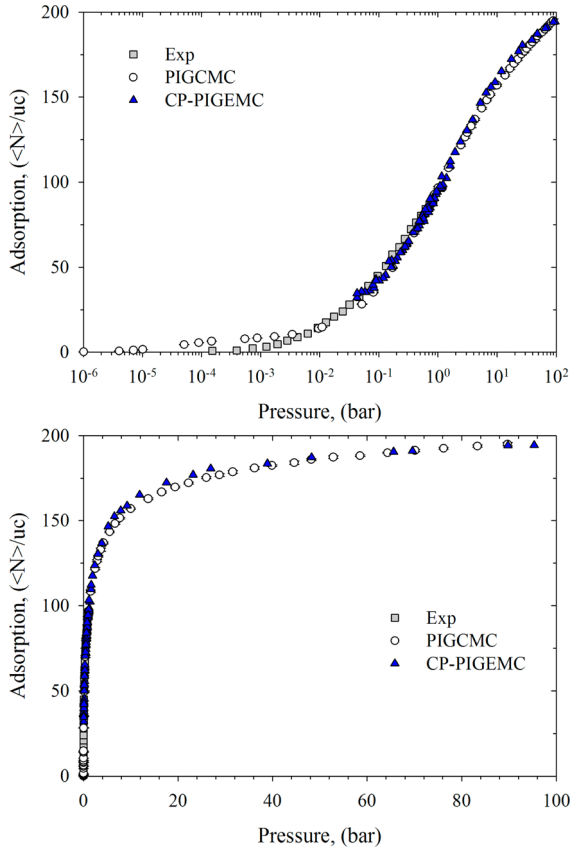

Figure 2. *Para*-H_2 absolute Gibbs adsorption isotherms in the NaX zeolite crystal at 77 K simulated by the PIGCMC (○) and CP-PIGEMC (▲). The experimental H_2 adsorption isotherm (■) covers the pressure range up to 1 bar, whereas theoretical isotherms computed from path integral Monte Carlo methods were simulated up to 10^2 bar.

theoretically (with both CP-PIGEMC and PIGCMC methods) and measured experimentally at 77 K. Additionally, we computed two adsorption *para*-H_2 isotherms in NaX zeolite from (NVT) MD simulations (see Figure 3). The first MD adsorption isotherm was computed for rigid NaX zeolite framework, whereas the second one was computed for mobile Na cations. We point out that experiment and theoretical isotherms computed from MD simulations cover the pressure range up to 1 bar, whereas theoretical isotherms computed from path integral Monte Carlo methods were simulated up to 10^2 bar. Extrapolation of experimental adsorption measurements to higher pressures by (NVT) MD simulation method implemented with Widom's particle insertion algorithm[39] is very difficult. For higher external bulk pressures, the efficiency of particle insertion into inhomogeneous and dense adsorbed *para*-H_2 fluid is very low. Therefore, PIGCMC and CP-PIGEMC algorithms are far more efficient tools for studying the high-pressure adsorption equilibrium of *para*-H_2 on NaX zeolite (see Figure 2). From the experiment, we found that the adsorption of *para*-H_2 at 77 K started at low pressures ($\sim 10^{-3}$ bar). The NaX zeolite framework was not saturated by adsorbed *para*-H_2 within the experimental pressure range.

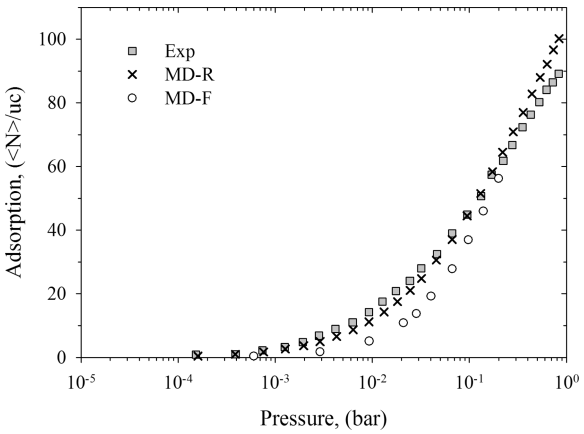

Figure 3. *Para*-H_2 absolute Gibbs adsorption isotherms in the NaX zeolite crystal at 77 K simulated by the canonical (NVT) molecular dynamics. Exp corresponds to the experimental H_2 adsorption isotherm, MD-R corresponds to rigid zeolite framework, and MD-F corresponds to rigid zeolite framework with mobile Na cations.

Finally, the experimental adsorption isotherm is a typical Langmuirian one (i.e., Type I according to the IUPAC[42] classification of physisorption isotherms) with convex curvature characteristics for adsorption systems where solid−fluid interactions are significantly higher than fluid−fluid ones. The agreement between the experimental and simulated adsorption isotherms is very good. We notice that PIGCMC generates small values of *para*-H_2 adsorption at pressures $\sim 10^{-4}$ bar. Crystal defects and other structural/energetic heterogeneities of the real NaX zeolite crystal may be responsible for observed differences at very low pressures (see the upper panel in Figure 2). Above pressures of $\sim 10^{-3}$ bar, the experimental adsorption isotherm is nicely reproduced by the theoretical isotherm computed from PIGCMC. For comparison, we simulated *para*-H_2 adsorption at 77 K and a pressure range $\sim 10^{-1}$−10^2 bar by our CP-PIGEMC algorithm. As expected, theoretical values of adsorbed amounts computed from PIGCMC and CP-PIGEMC are fully consistent. By extrapolation of experimental measurements to higher pressures, we found that the NaX zeolite is able to adsorb ∼195 *para*-H_2 molecules per unit cell at 99 bar at 77 K (see horizontal plateau on simulated isotherms that provide the nanopore capacity exactly).

Figure 4 presents the equilibrium CP-PIGEMC snapshot of *para*-H_2 molecules adsorbed in the NaX zeolite at 99 bar and 77 K. We stress that the amount of adsorbed *para*-H_2 at higher pressures and 77 K is difficult to access experimentally. Thus, the extrapolation of experimental results by our computer experiments not only gives unique insight into the packing of *para*-H_2 molecules in NaX zeolite cages but also allows precise calculation of *para*-H_2 storage. Not surprisingly, the volumetric density of adsorbed *para*-H_2 ∼40 g L^{-1} is far below the liquid density of *para*-H_2 at boiling point ∼ 71 g L^{-1}. Even at high operating pressures, adsorbed *para*-H_2 molecules are loosely packed in the NaX zeolite cages (see the bulk-like structures of adsorbed molecules shown in Figure 4). Weak electrostatic interactions generated from Na cations and short-range weak dispersion interactions between *para*-H_2 molecules and NaX zeolite framework atoms are responsible for the low densification of supercritical *para*-H_2 fluid. It is worth mentioning that the volumetric density of *para*-H_2 in ordinary carbonaceous materials at 1 bar and 77 K is ∼30−40 g L^{-1} (see ref 43). Clearly, exchange of Na cations by higher valence ones

dx.doi.org/10.1021/ct400110c | J. Chem. Theory Comput. XXXX, XXX, XXX−XXX

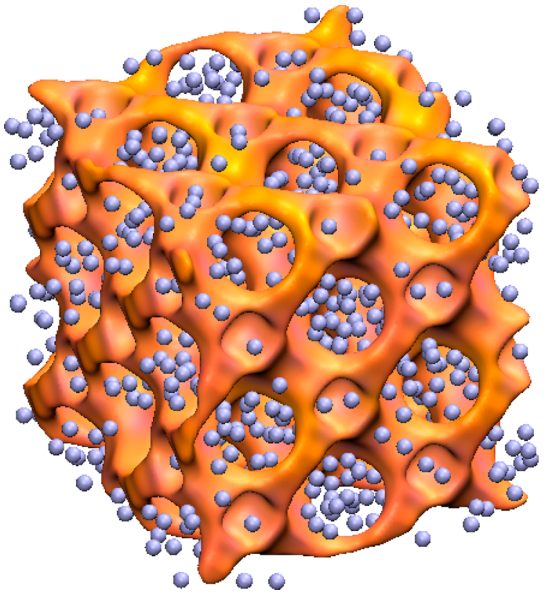

Figure 4. CP-PIGEMC snapshot of *para*-H_2 adsorbed in the NaX zeolite crystal ($Na_{85}Al_{86}Si_{106}O_{384}$) consisting of 8 unit cells at 99 bar and 77 K. Blue spheres denote the centroid positions of adsorbed *para*-H_2 molecules. Under the studied operating conditions, NaX zeolite crystal adsorbs 40.4 g L^{-1} (note that the volumetric density of liquid H_2 at the boiling point is 71 g L^{-1}).

(e.g., calcium, magnesium, chromium, etc.) should improve the binding of *para*-H_2. This interesting aspect of *para*-H_2 adsorption in zeolites is beyond the scope of our work.

It is instructive to see how the CP-PIGEMC simulation system approaches the thermodynamic equilibrium. For this case study, we selected an external pressure of *para*-H_2 equal to 11.9 bar, with random initial configurations of 4000 and 5 *para*-H_2 molecules in the bulk and pore cell, respectively (see Figure 5). Because the initial densities in these coupled cells are far from thermodynamic equilibrium, we observe continuous transport of *para*-H_2 molecules from the bulk to the pore cell, as is displayed in Figure 5. The simulated system stabilized around 8×10^6 CP-PIGEMC steps. Here, we observe statistical

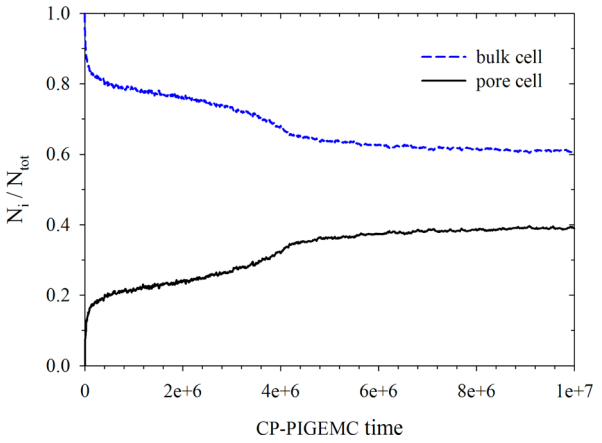

Figure 5. CP-PIGEMC time variation of the number of *para*-H_2 molecules, N_i/N_{tot}(where index '*i*' denotes selected simulation cell: 'p' or 'b'), in bulk and pore cell normalized by the total number of *para*-H_2 molecules ($N_{tot} = N_p + N_b$). Plots correspond to the adsorption of *para*-H_2 in the NaX zeolite crystal at 77 K and the external pressure of *para*-H_2 of 11.9 bar.

fluctuations of bulk cell volume around its equilibrium value. Obviously, to reduce the CP-PIGEMC simulation time, one can set up initial configurations of *para*-H_2 molecules in bulk and pore cell closer to thermodynamic equilibrium. The important point, however, is that the final thermodynamic equilibrium does not depend on the initial state of the bulk and pore cell (i.e., our CP-PIGEMC algorithm is ergodic).

The enthalpy released during *para*-H_2 adsorption in NaX zeolite at 77 K is nonmonotonic (see Figure 6). High enthalpy

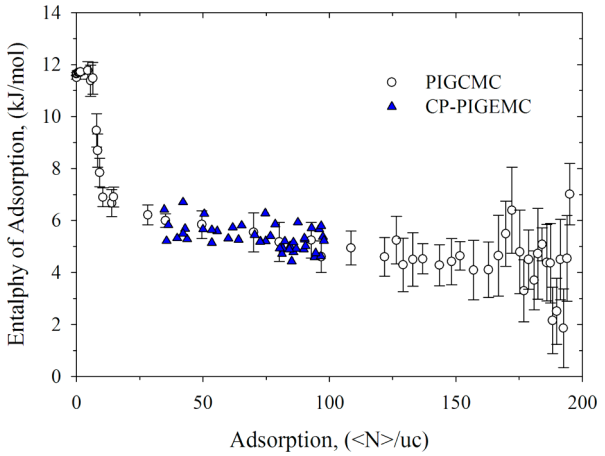

Figure 6. Enthalpies of adsorption per mole for *para*-H_2 adsorbed in the NaX zeolite crystal at 77 K simulated by the PIGCMC (○) and CP-PIGEMC method (▲).

realizes at zero coverage (~ 11.8 kJ mol^{-1}) decreases quickly with filling of the NaX zeolite by adsorbed *para*-H_2 molecules. Not surprisingly, the strongest adsorption sites in NaX zeolite (i.e., Na cations) are saturated at low nanopore loadings (i.e., around ~10 *para*-H_2 molecules in a unit cell). Further adsorption corresponds to the filling of large zeolite cages by *para*-H_2 molecules. These cages have significantly lower binding energy toward *para*-H_2 molecules. Moreover, the adsorbed *para*-H_2 molecules repeal one another because of compression (i.e., repulsive interactions in the adsorbed phase). Thus, overall, at higher loading of *para*-H_2, the adsorption enthalpy drops to ~4−5 kJ mol^{-1}, as is computed from both the PIGCMC and CP-PIGEMC algorithms (see Figure 6). The problem of how to strongly bind *para*-H_2 molecules at higher pore loadings must be addressed in order to get high storage of *para*-H_2.

Finally, the variation of the effective size of the path (i.e., radius of gyration) with filling of NaX zeolite by adsorbed *para*-H_2 molecules is shown in Figure 7. The average value of the radius of gyration of *para*-H_2 paths in bulk cell is ~0.277 Å (see bottom panel in Figure 7). Thus, as would be expected, confinement effects induce compression of adsorbed *para*-H_2 paths as compared to the bulk gaseous phase. More interestingly, we found that the effective size of confined *para*-H_2 paths is not constant but strongly depends on the density of the adsorbed fluid. At low nanopore densities (i.e., ~10−12 *para*-H_2 molecules per unit cell), adsorbed paths undergo strong compression (i.e., localization in positional space). This effect can be explained as strong binding of *para*-H_2 molecules to Na cations. With further adsorption (i.e., ~140−150 *para*-H_2 molecules per unit cell), we observe expansion of *para*-H_2 paths. This is not surprising because *para*-H_2 molecules adsorbed in NaX zeolite cages have more space

dx.doi.org/10.1021/ct400110c | J. Chem. Theory Comput. XXXX, XXX, XXX−XXX

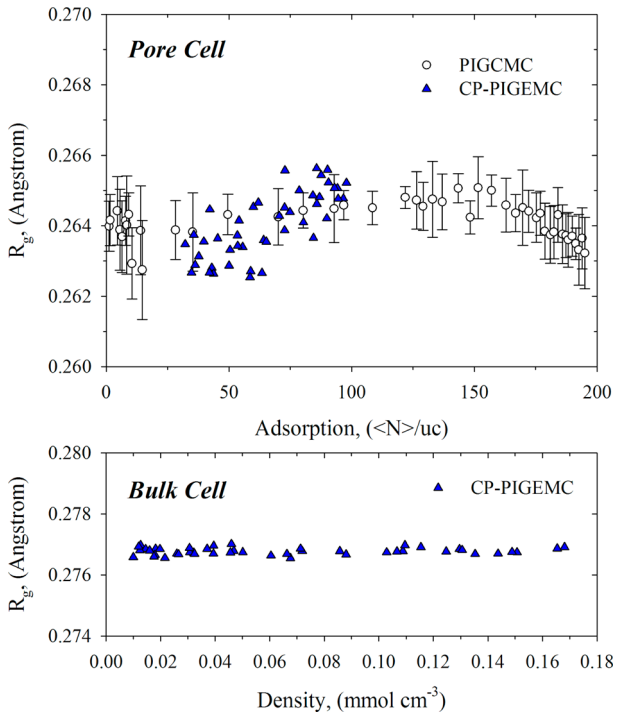

Figure 7. Upper panel: variations of radius of gyration with *para*-H_2 density in the NaX zeolite crystal at 77 K simulated by the PIGCMC (open circles) and CP-PIGEMC method (closed triangles). Bottom panel: variations of radius of gyration in the bulk cell with *para*-H_2 density at 77 K simulated by the CP-PIGEMC method.

for their delocalization. Interestingly, direct comparison of the radius of gyration computed in both simulation cells (i.e., for adsorbed phase and coexisting bulk fluid) reveals that *para*-H_2 molecules adsorbed in NaX zeolite cages are far more localized in positional space as in the bulk phase (see Figure 7). Finally, as the density of adsorbed fluid increases even further, the repulsive forces between confined *para*-H_2 paths induce stronger localization in positional space. That is why we observe compression of adsorbed paths around ~190 *para*-H_2 molecules per unit cell. As for other computed averages, CP-PIGEMC and PIGCMC results are fully consistent.

V. CONCLUSIONS

We have presented the extension of the constant pressure Gibbs ensemble Monte Carlo method for the simulation of one-component fluid consists of distinguishable quantum particles (*Boltzmannons*) in an external potential field at finite temperatures. Quantum effects (i.e., zero-point motion and tunneling) were captured by real-space Feynman path integral formalism. A novel constant pressure Gibbs ensemble path integral Monte Carlo (CP-PIGEMC) method was used for investigation of *para*-H_2 adsorption in NaX zeolite at 77 K. The CP-PIGEMC simulation results are in excellent agreement with experimental data and theoretical results computed from standard path integral grand canonical Monte Carlo method (PIGCMC). Extrapolation of experimental measurements to high pressures reveals that NaX zeolite is not a suitable nanoporous material for on-board *para*-H_2 storage. The volumetric density of *para*-H_2 adsorbed in NaX zeolite at 99 bar and 77 K is only ~40 g L^{-1} (note that liquid density of *para*-H_2 at boiling point ~71 g L^{-1}). From a practical point of view, CP-PIGEMC is a very useful method when the quantum fluid storage at a single external pressure (or several values of external pressures) needs to be predicted.

■ ASSOCIATED CONTENT

Supporting Information

N_2 adsorption−desorption isotherms in model cylindrical silica pores computed by the GCMC (open circles) and CP-GEMC method (closed squares) at 77.4 K (Figure 1S and 2S), and the Silvera-Goldman potential parameters (Table 1S). This material is available free of charge via the Internet at http://pubs.acs.org.

■ AUTHOR INFORMATION

Corresponding Author

*Tel.: +61 8 9266 7800. E-mail: Piotr.Kowalczyk@curtin.edu.au.

Notes

The authors declare no competing financial interest.

■ ACKNOWLEDGMENTS

P.K. acknowledges partial support by the Office of Research & Development, Curtin University of Technology, Grant CRF10084. P.G. and A.P. Terzyk acknowledge the use of the computer cluster at Poznan Supercomputing and Networking Centre and Networking Centre and the Information and Communication Technology Centre of the Nicolaus Copernicus University. P.K. acknowledges Prof. J. Gale (Curtin University of Technology, Australia) for fruitful discussions about molecular simulations of zeolites. P.K. would like to thank the discussions and hospitality of the Prof. D. Theodorou (National Technical University of Athens, Greece).

■ REFERENCES

(1) Feynman, R. P.; Hibbs, A. *Quantum Mechanics and Path Integrals*; McGraw- Hill: New York, 1965.
(2) Feynman, R. P. *Statistical Mechanics*; Benjamin: New York, 1972.
(3) Ceperley, D. M. Path Integrals in the Theory of Condensed Helium. *Rev. Mod. Phys.* **1995**, *67*, 279−356.
(4) Ceperley, D. M. Microscopic Simulations in Physics. *Rev. Mod. Phys.* **1999**, *71*, S438−S443.
(5) Tuckerman, M. E.; Marx, D.; Parrinello, M. The Nature and Transport Mechanism of Hydrated Hydroxide Ions in Aqueous Solution. *Nature* **2002**, *417*, 925−929.
(6) Wang, Q.; Johnson, J. K. Phase Equilibrium of Quantum Fluids from Simulation: Hydrogen and Neon. *Fluid Phase Equilib.* **1997**, *132*, 93−116.
(7) Rabani, E.; Krilov, G.; Reichman, D. R.; Berne, B. J. Transport Properties of Normal Liquid Helium: Comparison of Various Methodologies. *J. Chem. Phys.* **2005**, *123*, 184506−1−184506−7.
(8) Tuckerman, M. E.; Marx, D.; Klein, M. L.; Parrinello, M. On the Quantum Nature of the Shared Proton in Hydrogen Bonds. *Science* **1997**, *275*, 817−820.
(9) Morales, M. A.; Pierleoni, C.; Schwegler, E.; Ceperley, D. Phase Separation in Hydrogen-Helium Mixtures at Mbar Pressures. *Proc. Natl. Acad. Sci. U.S.A.* **2009**, *106*, 1324−1329.
(10) Kowalczyk, P.; Gauden, P. A.; Terzyk, A. P.; Bhatia, S. K. Thermodynamics of Hydrogen Adsorption in Slit-like Carbon Nanopores at 77 K. Classical Versus Path-Integral Monte Carlo Simulations. *Langmuir* **2007**, *23*, 3666−3672.
(11) Nakayama, A.; Makri, N. Simulation of Dynamical Properties of Normal and Superfluid Helium. *Proc. Natl. Acad. Sci. U.S.A.* **2005**, *102*, 4230−4234.
(12) Rabani, E.; Reichman, D. R.; Krilov, G.; Berne, B. The Calculation of Transport Properties in Quantum Liquids Using the Maximum Entropy Numerical Analytic Continuation Method:

Application to Liquid *para*-Hydrogen. *J. Proc. Natl. Acad. Sci. U.S.A.* **2002**, *99*, 1129−1133.
(13) Berne, B. J.; Thirumalai, D. On the Simulation of Quantum Systems: Path Integral Methods. *Annu. Rev. Phys. Chem.* **1986**, *37*, 401−424.
(14) Habershon, S.; Manolopoulos, D. E.; Markland, T. E.; Miller, T. F., III Ring Polymer Molecular Dynamics: Quantum Effects in Chemical Dynamics from Classical Trajectories in an Extended Phase Space. *Annu. Rev. Phys. Chem.* **2013**, *64*, 387−413.
(15) Miller, T. F., III Isomorphic Classical Molecular Dynamics Model for and Excess Electron in a Supercritical Fluid. *J. Chem. Phys.* **2008**, *129*, 194502−194512.
(16) Chandler, D.; Leung, K. Excess Electrons in Liquids: Geometrical Perspectives. *Annu. Rev. Phys. Chem.* **1994**, *45*, 557.
(17) Hone, T. D.; Voth, G. A. A Centroid Molecular Dynamics Study of Liquid *para*-Hydrogen and *ortho*-Deuterium. *J. Chem. Phys.* **2004**, *121*, 6412−6423.
(18) Wang, Q.; Challa, S. R.; Sholl, D. S.; Johnson, J. K. Quantum Sieving in Carbon Nanotubes and Zeolites. *Phys. Rev. Lett.* **1999**, *82*, 956−959.
(19) Wilner, E. Y.; Levy, T. J.; Rabani, E. Analytical Continuation Approaches to Electronic Transport: the Resonant Level Model. *J. Chem. Phys.* **2012**, *137*, 214107−214114.
(20) Kletenik-Edelman, O.; Reichman, D. R.; Rabani, E. On the Mode-Coupling Treatment of Collective Density Fluctuations for Quantum Liquids: *para*-Hydrogen and Normal Liquid Helium. *J. Chem. Phys.* **2011**, *134*, 044528−1−044528−10.
(21) Thirumalai, D.; Hall, R. W.; Berne, B. J. A Path Integral Monte Carlo Study of Liquid Neon and the Quantum Effective Pair Potential. *J. Chem. Phys.* **1984**, *81*, 2523−2527.
(22) Kowalczyk, P.; Gauden, P. A.; Terzyk, A. P.; Furmaniak, S. Frequency-Dependent Diffusion Constant of Quantum Fluids From path Integral Monte Carlo and Tikhonov's Regularizing Functional. *J. Chem. Theory Comput.* **2009**, *5*, 1990−1996.
(23) Wang, Q.; Johnson, J. K.; Broughton, J. Q. Path Integral Grand Canonical Monte Carlo. *J. Chem. Phys.* **1997**, *107*, 5108−5118.
(24) Kowalczyk, P.; Gauden, P. A.; Terzyk, A. P. Nanoporous Quantum Filters: Inside Vapor−Liquid Transitions of Quantum Fluids in Nanopores. *J. Phys. Chem. B* **2010**, *114*, 5047−5052.
(25) Chandler, D.; Wolynes, P. G. Exploiting the Isomorphism Between Quantum Theory and Classical Statistical Mechanics of Polyatomic Fluids. *J. Chem. Phys.* **1981**, *74*, 4078−4096.
(26) Neimark, A. V.; Vishnyakov, A. Gauge Cell Method for Simulation Studies of Phase Transitions in Confined Systems. *Phys. Rev. E* **2000**, *62*, 4611−4621.
(27) Neimark, A. V.; Vishnyakov, A. The Birth of a Bubble: A Molecular Simulation Study. *J. Chem. Phys.* **2005**, *122*, 054707−1−054707−10.
(28) Widom, B. Some Topics in the Theory of Fluids. *J. Chem. Phys.* **1963**, *39*, 2808−2812.
(29) Nicholson, D.; Parsonage, N. G. *Computer Simulation and the Statistical Mechanics of Adsorption*; Academic Press: London, 1982.
(30) McGrother, S. C.; Gubbins, K. E. Constant Pressure Gibbs Ensemble Monte Carlo Simulations of Adsorption Into Narrow Pores. *Mol. Phys.* **1999**, *97*, 955−965.
(31) Silvera, I. F.; Goldman, V. V. The Isotopic Intermolecular Potential for H_2 and D_2 in the Solid and Gas Phases. *J. Chem. Phys.* **1978**, *69*, 4209−4214.
(32) Bezus, A. G.; Kiselev, A. V.; Lopatkin, A. A.; Du, P. Q. Molecular Statistical Calculation of the Thermodynamic Adsorption Characteristics of Zeolites Using the Atom−Atom Approximation. Part 1. Adsorption of Methane by Zeolite NaX. *J. Chem. Soc. Faraday Trans. 2* **1978**, *74*, 367−379.
(33) Kiselev, A. V.; Du, P. Q. Molecular Statistical Calculation of the Thermodynamic Adsorption Characteristics of Zeolites Using the Atom−Atom Approximation. Part 2. Adsorption of Non-Polar and Polar Inorganic Molecules by Zeolites Types X and Y. *J. Chem. Soc. Faraday Trans. 2* **1981**, *77*, 1−15.
(34) Kiselev, A. V.; Du, P. Q. Molecular Statistical Calculation of the Thermodynamic Adsorption Characteristics of Zeolites Using the Atom−Atom Approximation. Part 3. Adsorption of Hydrocarbons. *J. Chem. Soc. Faraday Trans. 2* **1981**, *77*, 17−32.
(35) Pantatosaki, E.; Papadopoulos, G.; Jobic, H.; Theodorou, D. N. Combined Atomistic Simulation and Quasi-Elastic Neutron Scattering Study of the Low-Temperature Dynamics of Hydrogen and Deuterium Confined in NaX Zeolite. *J. Phys. Chem. B* **2008**, *112*, 11708−11715.
(36) Pantatosaki, E.; Papadopoulos, G. On the Computation of Long-Range Interactions in Fluids Under Confinement: Application to Pore Systems With Various Types of Spatial Periodicity. *J. Chem. Phys.* **2007**, *127*, 164723−164733.
(37) Allen, M. P.; Tildesley, D. J. *Computer Simulation of Liquids*; Clarendon: Oxford, 1987.
(38) Ungerer, Ph.; Tavitian, B.; Boutin, A. *Applications of Molecular Simulation in the Oil and Gas Industry. Monte Carlo Methods*; IFP Publications: Paris, 2005.
(39) Pantatosaki, E.; Jobic, H.; Kolokolov, D. I.; Karmakar, S.; Biniwale, R.; Papadopoulos, G. K. Probing the Hydrogen Equilibrium and Kinetics in Zeolite Imidazolate Frameworks via Molecular Dynamics and Quasi-Elastic Neutron Scattering Experiments. *J. Chem. Phys.* **2013**, *138*, 034706−034716.
(40) Barker, J. A. A Quantum-Statistical Monte Carlo Method; Path Integrals with Boundary Conditions. *J. Chem. Phys.* **1979**, *70*, 2914−2919.
(41) Kowalczyk, P.; Gauden, P. A.; Terzyk, A. P.; Furmaniak, S. Impact the Carbon Pore Size and Topology on the Equilibrium Quantum Sieving of Hydrogen Isotopes at Zero-Coverage and Finite Pressures. *J. Phys.: Condens. Matter* **2009**, *21*, 144210−1−144210−12.
(42) Sing, K. S. W.; Everett, D. H.; Haul, R. A. W.; Moscou, L.; Pierotti, R. A.; Rouquerol, J.; Siemieniewska, T. Reporting Physisorption Data for Gas/Solid Interface with Special Reference to the Determination of Surface Area and Porosity. *Pure Appl. Chem.* **1985**, *57*, 603−619.
(43) Kowalczyk, P.; Holyst, R.; Terzyk, A. P.; Gauden, P. A. A State of Hydrogen in Idealized Carbon Slit-Like Nanopores at 77 K. *Langmuir* **2006**, *22*, 1970−1972.